Mi *et al.*
Chinese Journal of Mechanical Engineering (2024) 37:52
https://doi.org/10.1186/s10033-024-01030-8

Chinese Journal of Mechanical Engineering

ORIGINAL ARTICLE

Open Access

Adaptive RISE Control of Winding Tension with Active Disturbance Rejection

Junjie Mi[1], Jianyong Yao[1*] and Wenxiang Deng[1]

Abstract

A winding system is a time-varying system that considers complex nonlinear characteristics, and how to control the stability of the winding tension during the winding process is the primary problem that has hindered development in this field in recent years. Many nonlinear factors affect the tension in the winding process, such as friction, structured uncertainties, unstructured uncertainties, and external interference. These terms severely restrict the tension tracking performance. Existing tension control strategies are mainly based on the composite control of the tension and speed loops, and previous studies involve complex decoupling operations. Owing to the large number of calculations required for this method, it is inconvenient for practical engineering applications. To simplify the tension generation mechanism and the influence of the nonlinear characteristics of the winding system, a simpler nonlinear dynamic model of the winding tension was established. An adaptive method was applied to update the feedback gain of the continuous robust integral of the sign of the error (RISE). Furthermore, an extended state observer was used to estimate modeling errors and external disturbances. The model disturbance term can be compensated for in the designed RISE controller. The asymptotic stability of the system was proven according to the Lyapunov stability theory. Finally, a comparative analysis of the proposed nonlinear controller and several other controllers was performed. The results indicated that the control of the winding tension was significantly enhanced.

Keywords Winding tension, Continuous robust integral of the sign of the error (RISE) control, Adaptive control, Disturbance compensation, Extended state observer (ESO), Tension control

1 Introduction

As actuation systems are required to be increasingly lightweight, it is becoming increasingly important to reduce the weight of the structure and increase the power-to-weight ratio. Fiber-reinforced materials are widely used in lightweight structural designs because they have significantly better material properties, such as density, elastic modulus, and tensile strength, than traditional metal materials. Filament winding technology [1] was introduced in the 1940s and is currently one of the most common production technologies [2, 3]. In the 1990s, multi-axis winding machines emerged, and the development of winding technology entered a new stage. With improvements in numerical control technology, position control in the winding process has advanced. However, owing to the complexity and strong nonlinearity of the tension generation mechanism, tension control during the winding process has always been a key factor affecting the control performance.

In 1998, Mathur et al. [4] proposed a relatively complete tension control model for the winding process and proposed a formula for the change in coil diameter over time. Baumgart et al. [5–7] first applied robust control to tension control in the winding process, taking into account the air entrainment effect, and used the Lyapunov function to prove its stability. In 2004, they proposed the use of the state observer method and verified its feasibility. They then studied the controller design of

*Correspondence:
Jianyong Yao
jerryyao.buaa@gmail.com
[1] School of Mechanical Engineering, Nanjing University of Science and Technology, Nanjing 210094, China

the winding process under finite-time stability. In 2007, Pagilla et al. [8] applied the partition concept to long-distance winding for the first time and established a mathematical model for the material between two guide wheels during the winding process for controller design. In 2013, Levine et al. [9] proposed the application of a combination of differential flattening and feedback linearization to a winding system and verified its feasibility. In 2016, Hou et al. [10] developed a robust tension observer for winding systems. Owing to the research methods proposed by these scholars, tension control has entered the nonlinear research stage; however, decoupling the speed loop and tension loop is difficult owing to the composite control of the rewinding/unwinding reel and the construction brought about by the partition concept of long-distance winding. The modular complexity significantly limits the application of additional algorithms.

Disturbances are an important part of the system model uncertainty. Since the 1990s, nonlinear algorithms have developed rapidly, and a nonlinear algorithm called sliding mode control (SMC) has been widely used because of its simple structure, effective handling of bounded model uncertainty, and good steady-state tracking accuracy. Owing to the discontinuity problem of traditional synovial control, many deformation forms of SMC have been derived, among which high-order SMC [11, 12] has attracted extensive attention. In recent years, the robust integral of the sign of the error (RISE) control strategy [13] was proposed, which incorporates an integral signal feedback term to deal with model uncertainty and has been successfully applied in mechatronic systems [14–17]. Additionally, the modeling uncertainty, which is the main factor affecting the control performance, has been widely studied. Lewis et al. [18] first proposed a method using neural-network approximation, in which the two-link manipulator is taken as the object to compensate for system disturbance during the control process of the manipulator, which provided a theoretical basis for the subsequent application of neural networks. The observer-based control concept proposed by Khalil [19] has been developed continuously in recent years. Disturbance observers can treat disturbances as additional states to approximate them and compensate for disturbances and other nonlinear terms [20–23]. In Ref. [20], an active disturbance rejection control (ADRC) strategy was used to address many uncertainties and additional perturbations in dynamics [24]. The core design principle of the ADRC is to use the extended state observer (ESO) to estimate disturbances and other uncertainty terms and compensate them using the feedforward method in the design control input, so that the tracking error is bounded and stable. Yao et al. [25–28] experimentally verified that ESO-based compensation can deal with external disturbances. The superiority of ESO for disturbance compensation processing has been proven in many academic studies [29–32]. Therefore, the ADRC strategy can effectively deal with various model uncertainties, including disturbances, if the ESO can estimate them accurately.

However, the aforementioned research methods simplify the model to different degrees and do not consider the nonlinear problems that exist in the actual winding process.

In this study, a mathematical model of a winding system considering continuous external disturbance and friction compensation was established. Compared with the traditional tension control model, it is simpler and does not require decoupling of the speed and tension loops. Meanwhile, by using the ESO to estimate and compensate for uncertainties such as disturbances, the control law based on the RISE controller is designed. The combination of the two makes the system asymptotically stable and yields a better control effect than the previous control algorithm. This simplifies the design process of the tension control and provides a theoretical basis for the practical application of additional algorithms.

2 Nonlinear Model of Winding System

The general structure of the winding system is shown in Figure 1. Generally, two servomotors drive the rewinding and unwinding shafts. By adjusting the difference between the linear speeds of the winding and unwinding ends of the two shafts, a displacement difference was generated, and an appropriate tension was generated to satisfy the production requirements. A flowchart of this is shown in Figure 2.

2.1 Model of Tension Loop

Tension is mainly generated by the displacement difference between the two ends of retraction and release. A typical unwinding rule for a material at the unwinding end is shown in Figure 3. The specific influence on the tension is shown in Figure 4. Because the fiber material is evenly arranged on the substrate from one end to the other during production, the material moves to the left and right during the unwinding process. Consequently, the length from the unwinding end to the wire guide changes during

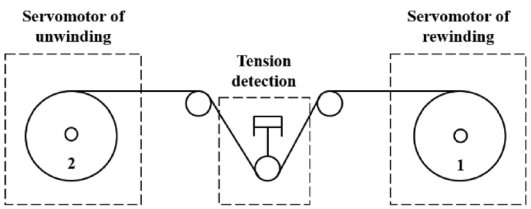

Figure 1 Structure diagram of the winding system

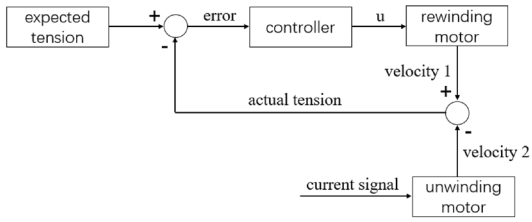

Figure 2 Winding tension control flowchart

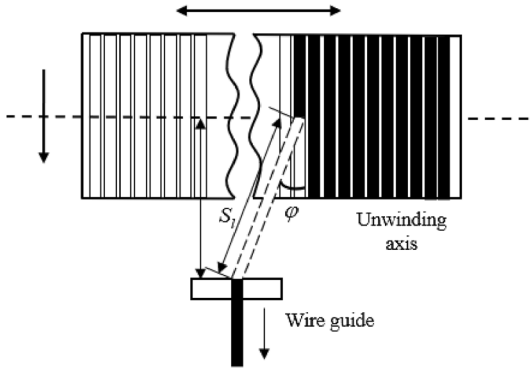

Figure 3 Lateral movement of the material causes the overall span length change

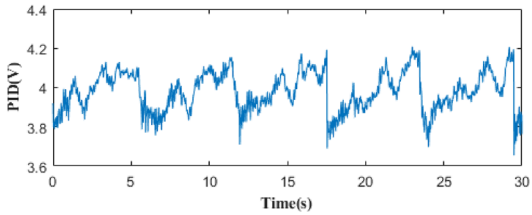

Figure 4 PID control input

unwinding, affecting the overall span length of the material, which influences the tension.

The tension model considering the length variation of the fiber material is expressed as follows [33]:

$$T(t,\omega_1) = \frac{EA}{S_0}S(t) + \boldsymbol{\Delta}_1(T,\omega_1,t), \tag{1}$$

$$S(t) = S_0 + \int_{t_0}^{t}(r_1\omega_1 - r_2\omega_2)\mathrm{d}\tau + S_l(t), \tag{2}$$

where r_i (m) and ω_i $(i = 1, 2)$ (rad/s) represent the rewinding and unwinding radius and angular velocity, respectively; E represents the elastic modulus of the material, A represents the cross-sectional area of the material, S_l represents the material length from the unwinding axis to the guide wire, S_0 represents the material length from the guide wire to the rewinding axis, $\boldsymbol{\Delta}_1(T,\omega_1,t)$ represents other unmodeled disturbances, and T represents the winding tension.

As shown in Figure 4, the control input range changes periodically as the span length changes. It was verified that the tension was mainly affected by the length of the material between the rewinding and unwinding axes, which affected the torque required by the rewinding shaft.

2.2 Model of Speed Loop

The winding system uses a motor as the main power source, which rotates the shaft to achieve winding. It is assumed that the speed of the unwinding shaft motor in this system is effectively controlled and can be measured. Therefore, the following mathematical model is established for the rewinding axis:

$$J\dot{\omega}_1 = K_i u - r_1 T - B\omega_1 - F_f(\omega_1) - \boldsymbol{\Delta}_2(\omega_1,t), \tag{3}$$

where K_i represents the voltage–torque coefficient, which is the amount of output torque per volt; J represents the inertia of the winding shaft; u represents the control law, which is generated by the controller and input to the actuator voltage signal; $F_f(\omega_1)$ denotes the static friction effect; B is the coefficient of viscous friction; and $\boldsymbol{\Delta}_2(\omega_1,t)$ represents disturbances.

The static friction effects are given by [15, 34]:

$$\begin{aligned} F_f(\omega_1) = {} & a_1 \tanh(c_1\omega_1) \\ & + a_2[\tanh(c_2\omega_1) - \tanh(c_3\omega_1)], \end{aligned} \tag{4}$$

where a_1 and a_2 represent friction levels, and c_1, c_2, c_3 are shape coefficients of various friction effects.

Remark 1 The friction model above is higher-order differentiable and symmetric with respect to velocity.

Remark 2 The Coulomb friction coefficient is modeled by the term $a_1\tanh(c_1\omega_1)$; the term $a_1 + a_2$ represents the stiction coefficient, and the term $\tanh(c_2\omega_1) - \tanh(c_3\omega_1)$ captures the Stribeck effect.

Considering Eq. (4), Eq. (3) can be rewritten as:

$$\begin{aligned} J\dot{\omega}_1 = {} & K_i u - r_1 T - B\omega_1 - a_1 S_f(\omega_1) \\ & - a_2 P_f(\omega_1) - \boldsymbol{\Delta}_2(\omega_1,t), \end{aligned} \tag{5}$$

where

$$\begin{aligned} S_f(\omega_1) &= \tanh(c_1\omega_1), \\ P_f(\omega_1) &= \tanh(c_2\omega_1) - \tanh(c_3\omega_1). \end{aligned} \tag{6}$$

2.3 State-Space Function of Winding Tension

We define $v_2 = r_2\omega_2$, $x = [x_1, x_2]^{\mathrm{T}} = [T, \omega_1]^{\mathrm{T}}$, $\theta_1 = EAr_1/S_0$, $\theta_2 = EAv_2/S_0$, $\theta_3 = K_i/J$, $\theta_4 = r_1/J$, $\theta_5 = B/J, \theta_6 = a_1/J, \theta_7 = a_2/J, \theta_{\mathrm{b}} = [\theta_4, \theta_5, \theta_6, \theta_7]^{\mathrm{T}}$, and $\eta = [x_1, x_2, S_{\mathrm{f}}, P_{\mathrm{f}}]^{\mathrm{T}}$. Therefore, the system can be expressed as the following state-space function:

$$\begin{aligned} \dot{x}_1 &= \theta_1 x_2 - \theta_2 + d_1(t), \\ \dot{x}_2 &= \theta_3 u - \theta_{\mathrm{b}}^{\mathrm{T}}\eta + d_2(t), \end{aligned} \tag{7}$$

where $d_1(t) = EA\dot{S}_l(t)/S_0 + \dot{\boldsymbol{\Delta}}_1(T, \omega_1, t)$ and $d_2(t) = \boldsymbol{\Delta}_2(\omega_1, t)$.

Assumption 1 $\boldsymbol{\Delta}_1(T, \omega_1, t)$ can be differentiated.

Assumption 2 $d_1(t)$ and $d_2(t)$ are bounded.

3 Design of Extended State Observers

Considering Eq. (7), traditional ESO designs observers according to the state-space equation structure of series integration; thus, only one observer is used for a system. Because all the system states are known, when a system needs to observe two external disturbances, two ESO observers can be designed to deal with relative uncertainties. We define $x_{\mathrm{e}1} = d_1(t)$ and $x_{\mathrm{e}2} = d_2(t)$ as additional state variables. Let $h_1(t)$ and $h_2(t)$ be the rates of change of the uncertainty, i.e., $\dot{x}_{\mathrm{e}1} = h_1(t)$ and $\dot{x}_{\mathrm{e}2} = h_2(t)$. Eq. (7) can be described as:

$$\begin{cases} \dot{x}_1 = \theta_1 x_2 - \theta_2 + x_{\mathrm{e}1}, \\ \dot{x}_{\mathrm{e}1} = h_1(t), \end{cases} \quad \begin{cases} \dot{x}_2 = \theta_3 u - \theta_{\mathrm{b}}^{\mathrm{T}}\eta + x_{\mathrm{e}2}, \\ \dot{x}_{\mathrm{e}2} = h_2(t). \end{cases} \tag{8}$$

Assumption 3 $h_1(t)$ and $h_2(t)$ are unknown but bounded functions.

From the ESO-based system model, i.e., Eq. (8), we observe that two state observers can be constructed as follows, referring to [26]:

$$\begin{cases} \dot{\hat{x}}_1 = \theta_1 x_2 - \theta_2 + \hat{x}_{\mathrm{e}1} + 2\omega_{\mathrm{o}1}(x_1 - \hat{x}_1), \\ \dot{\hat{x}}_{\mathrm{e}1} = \omega_{\mathrm{o}1}^2(x_1 - \hat{x}_1), \end{cases} \quad \begin{cases} \dot{\hat{x}}_2 = \theta_3 u - \theta_{\mathrm{b}}^{\mathrm{T}}\eta + \hat{x}_{\mathrm{e}2} + 2\omega_{\mathrm{o}2}(x_2 - \hat{x}_2), \\ \dot{\hat{x}}_{\mathrm{e}2} = \omega_{\mathrm{o}2}^2(x_2 - \hat{x}_2), \end{cases} \tag{9}$$

where $\hat{x}_i$ represents the estimate of x_i $(i = 1, 2)$, $\tilde{x}_i = x_i - \hat{x}_i$ represents the estimation errors, $\hat{x}_{ei}$ $(i = 1, 2)$ represents the estimates of the extended system states, x_{ei} and $\tilde{x}_{ei} = x_{ei} - \hat{x}_{ei}$ represent the estimation errors, and $\omega_{oi} > 0$ is the tuning parameter of the ESO observer bandwidth.

The choice of the polynomial coefficients in Eq. (9) is given by Refs. [26] and [35].

$$\lambda_{\mathrm{o}}(s) = (s + \omega_{\mathrm{o}})^2. \tag{10}$$

From Eq. (9), the first ESO is constructed according to the first rather than the second equation of Eq. (7). However, from an application perspective, the inherent disturbance of the tension loop is an obstacle to nonlinear control, and the state estimation of the second equation of Eq. (7) by the ESO is driven by the velocity signal, which contains measurement noise—particularly in practice. Therefore, the disturbance estimation of the velocity loop may be affected.

From Eqs. (8) and (9), the observer estimation error can be expressed as:

$$\begin{cases} \dot{\tilde{x}}_1 = \tilde{x}_{\mathrm{e}1} - 2\omega_{\mathrm{o}1}\tilde{x}_1, \\ \dot{\tilde{x}}_{\mathrm{e}1} = h_1(t) - \omega_{\mathrm{o}1}^2\tilde{x}_1, \end{cases} \quad \begin{cases} \dot{\tilde{x}}_2 = \tilde{x}_{\mathrm{e}2} - 2\omega_{\mathrm{o}2}\tilde{x}_2, \\ \dot{\tilde{x}}_{\mathrm{e}2} = h_2(t) - \omega_{\mathrm{o}2}^2\tilde{x}_2. \end{cases} \tag{11}$$

We define the following variables:

$$\begin{cases} \varepsilon = [\varepsilon_1, \varepsilon_2]^{\mathrm{T}} = \left[\tilde{x}_1, \dfrac{\tilde{x}_{\mathrm{e}1}}{\omega_{\mathrm{o}1}}\right]^{\mathrm{T}}, \\ \gamma = [\gamma_1, \gamma_2]^{\mathrm{T}} = \left[\tilde{x}_2, \dfrac{\tilde{x}_{\mathrm{e}2}}{\omega_{\mathrm{o}2}}\right]^{\mathrm{T}}. \end{cases} \tag{12}$$

The state estimation error dynamics can be given as:

$$\begin{cases} \dot{\varepsilon} = \omega_{\mathrm{o}1}A_1\varepsilon + B_1\dfrac{h_1(t)}{\omega_{\mathrm{o}1}}, \\ \dot{\gamma} = \omega_{\mathrm{o}2}A_2\gamma + B_2\dfrac{h_2(t)}{\omega_{\mathrm{o}2}}, \end{cases} \tag{13}$$

where

$$\begin{aligned} A_1 = A_2 &= \begin{bmatrix} -2 & 1 \\ -1 & 0 \end{bmatrix}, \\ B_1 = B_2 &= \begin{bmatrix} 0 \\ 1 \end{bmatrix}. \end{aligned} \tag{14}$$

Here, A_1 and A_2 are Hurwitz matrices, and the two positive matrices P_1 and P_2 satisfy the Lyapunov equation $A_i^{\mathrm{T}}P_i + P_iA_i = -I$, where I is an identity matrix.

Lemma 1 [35]: Considering Assumption 3, the estimated states are always bounded. Meanwhile, there exist two constants $\sigma > 0$ and $\upsilon > 0$ such that if the time

$T > 0$, c and a greater than 0 in finite time satisfy the following equation.

$$|\tilde{x}_j| \le \sigma, \sigma = O\left(\frac{1}{\omega_{o1}^{c}}\right), j = 1, \forall t \ge T, \tag{15}$$

$$|\tilde{x}_l| \le \upsilon, \upsilon = O\left(\frac{1}{\omega_{o2}^{a}}\right), l = 2, \forall t \ge T. \tag{16}$$

According to the main analysis in Ref. [35], it can be known that the construction of the ESOs in Eq. (9) stabilizes, and the estimation error of the expansion state can approach zero when the values of the parameters ω_{o1} and ω_{o2} are increased. Thus, the closed-loop stability is proven.

4 Design of Adaptive Rise Controller

4.1 Control Target

The target of the control is to maintain the winding tension at a constant value, which is denoted as x_{1d}. The tension tracking error e_1 is defined as follows:

$$e_1 = x_1 - x_{1d}. \tag{17}$$

Assumption 4 The desired tension trajectory x_{1d} is second-order derivable and bounded.

According to Assumption 1, we define:

$$\begin{aligned} r &= \dot{e}_1 + k_1 e_1, \\ e_2 &= x_2 - \alpha_1, \end{aligned} \tag{18}$$

where k_1 is a positive constant, α_1 denotes the virtual control law for x_2, e_2 represents the error between x_2 and α_1, and r represents the additional error signal.

4.2 Controller Design

According to Eqs. (8), (17), and (18), the error r can be expressed as:

$$\begin{aligned} r &= \dot{e}_1 + k_1 e_1 \\ &= \dot{x}_1 - \dot{x}_{1d} + k_1 e_1 \\ &= \theta_1 x_2 - \theta_2 + x_{e1} - \dot{x}_{1d} + k_1 e_1 \\ &= \theta_1 e_2 - \theta_2 + x_{e1} - \dot{x}_{1d} + k_1 e_1 + \theta_1 \alpha_1, \end{aligned} \tag{19}$$

sign(•) denotes the standard signum function, which is expressed as:

$$\text{sign}(\bullet) = \begin{cases} 1, & \text{if} \bullet \ge 0, \\ -1, & \text{if} \bullet < 0, \end{cases} \tag{20}$$

and the virtual control law α_1 can be designed as:

$$\alpha_1 = \alpha_{1a} + \alpha_{1s}, \quad \alpha_{1s} = \alpha_{1s1} + \alpha_{1s2}, \tag{21}$$

$$\begin{aligned} \alpha_{1a} &= \frac{1}{\theta_1}\left[\theta_2 - \hat{x}_{e1} + \dot{x}_{1d} - k_1 e_1\right], \quad \alpha_{1s1} = -\frac{1}{\theta_1} k_r e_1, \\ \alpha_{1s2} &= -\frac{1}{\theta_1}\int_0^t \left[k_r k_1 e_1 + \hat{\beta}\,\text{sign}(e_1)\right] \mathrm{d}\tau, \end{aligned} \tag{22}$$

where $k_r > 0$ is a positive feedback gain; the function of α_{1a} is a model compensation term; α_{1s} and α_{1s1} represent the robust and linear robust feedback laws, respectively; and α_{1s2} is a RISE term. $\hat{\beta}$ represents an estimated robust feedback gain, and the function is updated as

$$\dot{\hat{\beta}} = \gamma r \,\text{sign}(e_1), \tag{23}$$

where $\gamma > 0$ represents an adaptation gain. α_{1s2} is to compensate for modeling uncertainties by appropriately selecting adaptive gains.

According to Eqs. (21) and (22), Eq. (19) can be rewritten as follows:

$$r = \theta_1 e_2 + \theta_1 \alpha_{1s2} + \tilde{x}_{e1} - k_r e_1. \tag{24}$$

Considering Eq. (21) and $\dot{e}_2 = \dot{x}_2 - \dot{\alpha}_1$, differentiating r with respect to time yields:

$$\begin{aligned} \dot{r} &= \theta_1 \dot{e}_2 + \dot{\tilde{x}}_{e1} - k_r \dot{r} - \dot{\hat{\beta}}\,\text{sign}(e_1) \\ &= \theta_1 \dot{x}_2 - \theta_1 \dot{\alpha}_1 + \dot{\tilde{x}}_{e1} - k_r \dot{r} - \dot{\hat{\beta}}\,\text{sign}(e_1) \\ &= \theta_1 \theta_3 u - \theta_1 \theta_b^{\mathrm{T}} \eta + \theta_1 x_{e2} \\ &\quad - \theta_1 \dot{\alpha}_1 + \dot{\tilde{x}}_{e1} - k_r \dot{r} - \dot{\hat{\beta}}\,\text{sign}(e_1). \end{aligned} \tag{25}$$

According to Eq. (25), the controller u can be defined as:

$$u = u_a + u_s, \quad u_s = u_{s1} + u_{s2}, \tag{26}$$

$$\begin{aligned} u_a &= \frac{1}{\theta_1 \theta_3}\left[\theta_1 \theta_b^{\mathrm{T}} \eta - \theta_1 \hat{x}_{e2} + \theta_1 \dot{\alpha}_1\right], \quad u_{s1} = -k_2 e_2, \\ u_{s2} &= -\frac{1}{\theta_1 \theta_3} \hat{\varphi}\,\text{sign}(e_2 + r), \end{aligned} \tag{27}$$

where k_2 represents the positive feedback gain. A discontinuous projection can be given as:

$$\text{Proj}(\bullet) = \begin{cases} 0, & \text{if } \hat{\varphi} = \varphi_{\max} \text{ and } \bullet > 0, \\ 0, & \text{if } \hat{\varphi} = \varphi_{\min} \text{ and } \bullet < 0, \\ \bullet, & \text{otherwise}, \end{cases} \tag{28}$$

φ is bounded, and the function is updated as:

$$\dot{\hat{\varphi}} = \text{Proj}[\kappa(e_2 + r)], \tag{29}$$

where $\kappa > 0$ is an adaptation gain and

$$\dot{\alpha}_1 = \dot{\alpha}_{1a} + \dot{\alpha}_{1s},\ \dot{\alpha}_{1s} = \dot{\alpha}_{1s1} + \dot{\alpha}_{1s2}, \tag{30}$$

$$\dot{\alpha}_{1a} = \frac{1}{\theta_1}\left[\theta_2 - \dot{\hat{x}}_{e1} + \ddot{x}_{1d} - k_1\dot{e}_1\right],\ \dot{\alpha}_{1s1} = -\frac{1}{\theta_1}k_r\dot{e}_1,$$
$$\dot{\alpha}_{1s2} = -\frac{1}{\theta_1}\left[k_r k_1 e_1 + \hat{\beta}\mathrm{sign}(e_1)\right]. \tag{31}$$

Substituting Eqs. (26) and (27) into Eq. (25) yields:

$$\dot{r} = -k_r r - k_2 e_2 + \theta_1\tilde{x}_{e2} + \dot{\hat{x}}_{e1} - \hat{\varphi}\mathrm{sign}(e_2 + r) - \hat{\beta}\mathrm{sign}(e_1). \tag{32}$$

From Eqs. (25) and (32), $\dot{e}_2$ is expressed as:

$$\theta_1\dot{e}_2 = -k_2 e_2 + \theta_1\tilde{x}_{e2} - \hat{\varphi}\mathrm{sign}(e_2 + r). \tag{33}$$

4.3 Stability Analysis

Considering Eqs. (23) and (29), we select the proper feedback gains k_1, k_2, and k_r and select β according to Lemma 2. The control law of Eq. (26) guarantees that the tension tracking error is regulated and that all the system signals are bounded.

$$e_1 \to 0 \quad \text{as} \quad t \to \infty. \tag{34}$$

Lemma 2 The function $L(t)$ can be designed as:

$$L(t) = r[N - \beta\mathrm{sign}(e_1)], \tag{35}$$

where $N = -r\dot{\tilde{x}}_{e1}$, and N is sufficiently smooth.

Assumption 5

$$|N| \le \xi_1, \quad |\dot{N}| \le \xi_2 0. \tag{36}$$

If we can select β to satisfy the inequality

$$\beta \ge \xi_1 + \frac{1}{k_1}\xi_2, \tag{37}$$

the following defined function $P(t)$ is always positive:

$$P(t) = \beta|e_1(0)| - e_1(0)N(0) - \int_0^t L(\tau)\mathrm{d}\tau. \tag{38}$$

Proof See Appendix A.

We define a Lyapunov function as:

$$V = \frac{1}{2}\left(e_1^2 + \theta_1 e_2^2 + r^2 + \gamma^{-1}\tilde{\beta}^2 + \kappa^{-1}\tilde{\varphi}^2 + 2P\right). \tag{39}$$

Lemma 3 If the adaptation gain β is positive, the inequality in Eq. (37) is satisfied, and the feedback is selected appropriately, the matrix Λ_1 is positive-definite.

$$\Lambda_1 = \begin{bmatrix} k_1 & -\frac{1}{2} & 0 \\ -\frac{1}{2} & k_r & \frac{1}{2} \\ 0 & \frac{1}{2} & k_2 \end{bmatrix}. \tag{40}$$

Proof See Appendix B.

Then, Eq. (34) can be satisfied under closed-loop conditions.

Remark 3 Lemma 3 implies that the controller proposed in Eq. (26) can bring the system into an asymptotically stable state.

5 Comparative Experimental Results

5.1 Experimental Setup

The validation testbed used to demonstrate the proposed controller design is shown in Figure 5. In this experimental platform, the rewinding and unwinding axes were driven by servomotors 1 and 2, respectively. The tension-detection module is shown in Figure 6. The servomotors were Kollmorgen AKM24D-ACBNAA-00 with a rated current of 2.21 A, rated torque of 1.41 N·m, and maximum velocity of 8000 r/min. The Heidenhain ERN 480 rotary encoder has a line count of approximately 2048. The measuring amplitude of the tension sensor was 50 N, and the accuracy was approximately 0.1%. The measurement and control software were used with a 16-bit analog/digital (A/D) transition board (Advantech PCI-1716), which collected the tension signal; a 16-bit counter card (Heidenhain IK-220), which collected the position signals of the rewinding and unwinding axes; and a 16-bit digital/analog (D/A) transition board (Advantech PCI-1723). The sampling time was 0.5 ms. The speed signal was obtained by differentiating the derivative of the

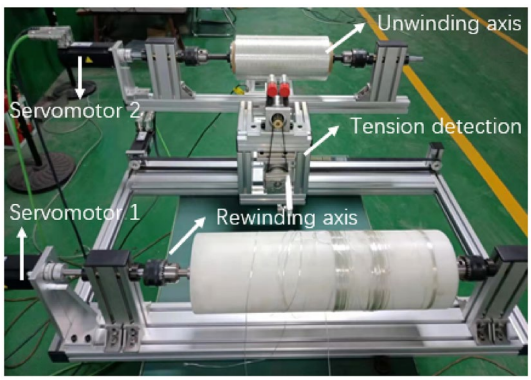

Figure 5 Experimental platform for winding tension

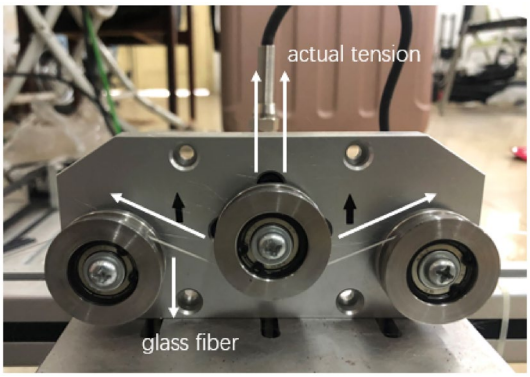

Figure 6 Detection module for winding tension

Table 1 Parameters of the winding system

Parameter	Value
Young's modulus E (N/m^2)	1.6×10^{9}
Material cross-sectional area A (m^2)	1.2×10^{-6}
Material span S_0 (m)	1.8
Velocity of unwinding v_2 (m/s)	8×10^{-2}
Radius of rewinding r_1 (m)	7.4×10^{-2}
Equivalent inertia J (kg · m^2)	6.3×10^{-3}
Voltage–torque coefficient K_i (N · m/V)	3.2×10^{-2}
Viscous friction coefficient B	1.3×10^{-1}
Friction levels a_1, a_2	0.02, 0.01
Corresponding coefficients c_1, c_2, c_3	500, 15, 1.5

high-precision position signal. The parameters of the winding system are presented in Table 1.

5.2 Comparative Experimental Results

To demonstrate the advantages of the proposed controller, we compared it with three other controllers.

(1) ESOARISE

The control gains were selected as $k_1 = 20$, $k_r = 6$, and $k_2 = 10$. The observer bandwidth parameter was set as $\omega_{o1} = 30$ and $\omega_{o2} = 20$. The adaptation rates of the parameters were set as $\gamma = 5$ and $\kappa = 1$.

(2) ARISE

The input of adaptive RISE control is:

$$u = \frac{1}{\theta_1\theta_3}\left[\theta_1\theta_b^{\mathrm{T}}\eta + \theta_1\dot{\alpha}_1 - k_2e_2\right]. \tag{41}$$

The virtual control law α_1 in Eq. (41) is:

$$\alpha_1 = \frac{1}{\theta_1}[\theta_2 + \dot{x}_{1d} - k_1e_1 - k_re_1] - \frac{1}{\theta_1}\int_0^t \left[k_rk_1e_1 + \hat{\beta}\mathrm{sign}(e_1)\right]\mathrm{d}\tau. \tag{42}$$

The control gains are identical to those of ESOARISE.

(3) RISE

The control law of RISE is:

$$u = \frac{1}{\theta_1\theta_3}\left[\theta_1\theta_b^{\mathrm{T}}\eta + \theta_1\dot{\alpha}_1 - k_2e_2\right], \tag{43}$$

and the virtual control law α_1 in Eq. (43) is:

$$\alpha_1 = \frac{1}{\theta_1}[\theta_2 + \dot{x}_{1d} - k_1e_1 - k_re_1] - \frac{1}{\theta_1}\int_0^t [k_rk_1e_1 + \beta\mathrm{sign}(e_1)]\mathrm{d}\tau. \tag{44}$$

The RISE feedback gain is $\beta = 350$, and the control gains and winding system parameters are identical to those in ESOARISE.

(4) PID

Proportional–integral–derivative (PID) controllers are widely used in engineering. The PID gains are selected as $k_p = 15$, $k_i = 8$, and $k_d = 0$.

In practical applications, the tension should be stable. The proposed controllers were run with a tension trajectory given by:

$$x_{1d} = 10\left(1 - e^{-t}\right), \tag{45}$$

which ensured that x_{1d} increased slowly from 0 to a constant value without mutation and was sufficiently smooth.

The tension tracking errors and actual tension signals of ESOARISE, ARISE, RISE, and PID are shown in Figures 7 and 8, respectively. The control input u for the four controllers is shown in Figure 9. The velocity of the rewinding axis is shown in Figure 10. The estimations of x_{e1} and x_{e2} are shown in Figure 11. The root-mean-square (RMS) values of each controller are presented in Table 2. In addition to the graph with the tracking error, the curves of physical quantities such as the actual tension, input voltage, and velocity of the rewinding are presented. The actual tension curve reflects the tension tracking performance, and the stability of the rewinding speed largely determines the accuracy of the

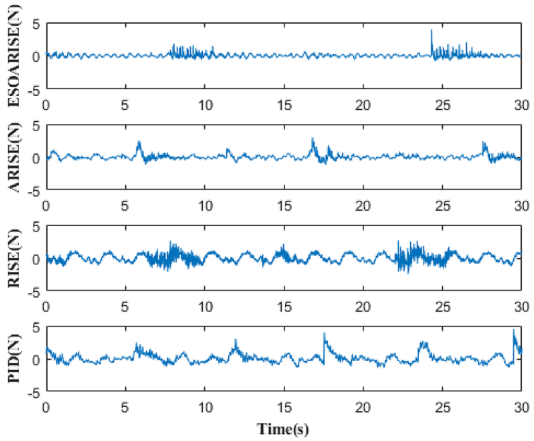

Figure 7 Tension tracking errors of the four controllers

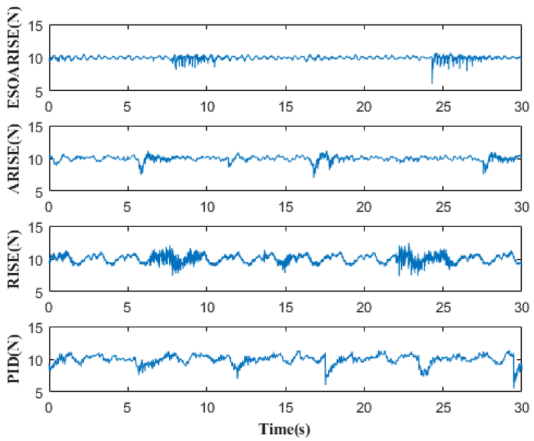

Figure 8 Actual tension values of the four controllers

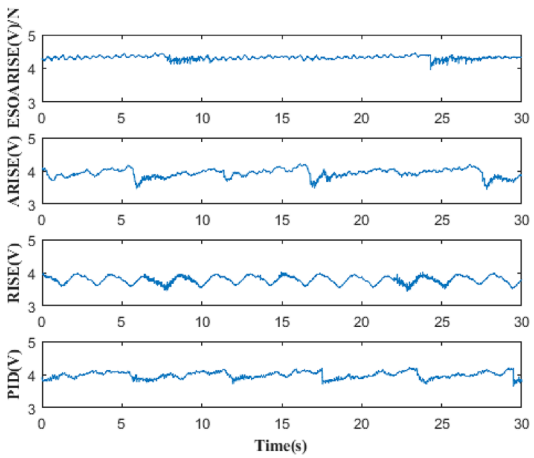

Figure 9 Control input voltages of the four controllers

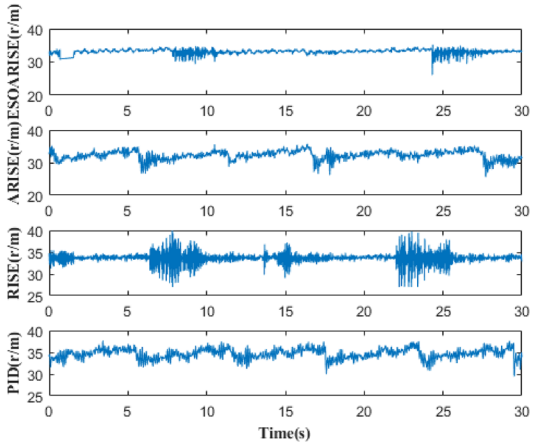

Figure 10 Velocity of the rewinding axis for the four controllers

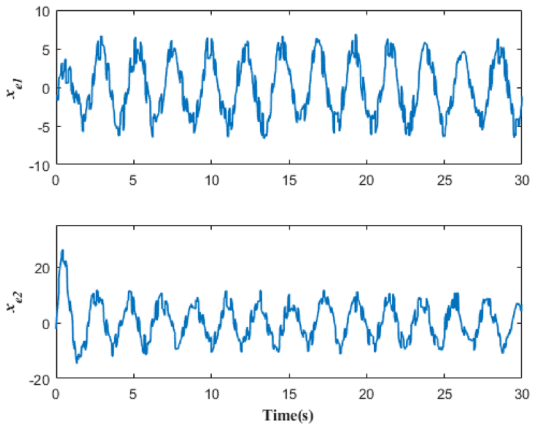

Figure 11 Disturbance estimation of the ESOARISE controller

Table 2 RMS values of the controllers

Controller	Value
ESOARISE	0.2507
ARISE	0.3918
RISE	0.6079
PID	0.6967

tension control. Finally, the input voltage represents the amplitude of the electrical signal required by the system to achieve accurate control.

In Figure 7, we can intuitively observe the tracking effect of each controller on the tension. As shown, ESOARISE had the best control effect among all the

controllers, and the PID controller had the worst control effect.

In addition, Figure 7 shows that RISE had better tracking performance than PID, confirming the effectiveness of the utilized nonlinear model and integral robust terms.

The tracking error of ARISE was more stable than that of RISE, verifying the effectiveness of the improvement of robust gain adaptation for the global tracking performance.

ESOARISE outperformed the other controllers in all aspects, as shown in Figures 7, 8, 9, 10. In particular, it was significantly better with regard to angular velocity and tension tracking error, verifying the effectiveness of disturbance compensation in the control law based on the ESO. The values of disturbances compensation are presented in Figure 11.

In Table 2, the values of ESOARISE are better than those of the other controllers, confirming the effectiveness and advanced nature of the proposed controller at the data level.

6 Conclusions

For a typical winding system, we considered the influence of the material length change between the rewinding and unwinding ends on the system tension as a time-varying interference term and reestablished the mathematical model of the winding system accordingly. An ESO was used to estimate the time-varying interference term, which was designed according to the continuous RISE method, and the parameter adaptive concept was used as the online update method for robust gain. The asymptotic stability of the system was verified using the Lyapunov function.

(1) Through a test analysis, with consideration of the linear velocity at the end of the unwinding reel as a known state, the state-space equation is redesigned, making it more convenient for the application of nonlinear algorithms. Compared with other control methods, the proposed method based on the ESO suppresses the interference to the winding tension caused by disturbances and increases the control accuracy for the tension of the winding system. Thus, it provides a theoretical basis for the development of tension control.

(2) However, this study had limitations. For example, only the control of the rewinding speed was considered, and the unwinding speed was assumed to be constant. Therefore, the improvement in the control performance was limited. In addition, the structural stability of glass fiber materials is poor, leading to errors and low consistency in the experimental results. Therefore, our future research will focus on model completeness and material selection.

Appendix A

To ensure the positive definiteness of the Lyapunov function (Eq. (39)) while guaranteeing the negative-definiteness of the Lyapunov-function differential, an auxiliary function $P(t) > 0$ must be designed to eliminate redundant terms, that is, $N = -r\dot{\tilde{x}}_{e1}$ and $\hat{\beta}\text{sign}(e_1)$. This is defined as $P(t)$ in Eq. (38), where

$$\begin{aligned}\int_0^t L(\tau)\mathrm{d}\tau &= \int_0^t r[N - \beta\text{sign}(e_1)]\mathrm{d}\tau \\ &= \int_0^t (\dot{e}_1 + k_1 e_1)[N - \beta\text{sign}(e_1)]\mathrm{d}\tau.\end{aligned} \tag{46}$$

Through integration by parts, Eq. (35) can be rewritten as follows:

$$\begin{aligned}\int_0^t L(\tau)\mathrm{d}\tau &= e_1 N|_0^t - \beta|e_1||_0^t \\ &\quad + \int_0^t k_1 e_1\left[N - \frac{1}{k_1}\dot{N} - \beta\text{sign}(e_1)\right]\mathrm{d}\tau \\ &= \beta|e_1(0)| - e_1(0)N(0) + e_1 N - \beta|e_1| \\ &\quad + \int_0^t k_1 e_1\left[N - \frac{1}{k_1}\dot{N} - \beta\text{sign}(e_1)\right]\mathrm{d}\tau,\end{aligned} \tag{47}$$

where the constant terms $\beta|e_1(0)|$ and $e_1(0)N(0)$ can be compensated in $P(t)$. Substituting Eq. (47) into Eq. (38) yields:

$$P(t) = \beta|e_1| - e_1 N - \int_0^t k_1 e_1\left[N - \frac{1}{k_1}\dot{N} - \beta\text{sign}(e_1)\right]\mathrm{d}\tau. \tag{48}$$

Considering Eq. (36), we can ensure that $P(t) > 0$ is always satisfied when β is designed as given by Eq. (37).

Appendix B

The time derivative of Eq. (39) can be expressed as:

$$\dot{V} = e_1\dot{e}_1 + e_2\theta_1\dot{e}_2 + r\dot{r} + \tilde{\beta}\gamma^{-1}\dot{\hat{\beta}} + \tilde{\varphi}\kappa^{-1}\dot{\hat{\varphi}} + P. \tag{49}$$

Substituting Eqs. (18), (23), (29), (32), and (33) into Eq. (49) yields:

$$\begin{aligned}\dot{V} &= e_1(r - k_1 e_1) + e_2\left[-k_2 e_2 + \theta_1\tilde{x}_{e2} - \hat{\varphi}\text{sign}(e_2 + r)\right] \\ &\quad + r\left[-k_r r - k_2 e_2 + \theta_1\tilde{x}_{e2} + \dot{\tilde{x}}_{e1}\right] \\ &\quad + r\left[-\hat{\varphi}\text{sign}(e_2 + r) - \hat{\beta}\text{sign}(e_1)\right] \\ &\quad + \tilde{\beta}r\text{sign}(e_1) + \tilde{\varphi}\text{Proj}(e_2 + r) \\ &\quad - r[N - \beta\text{sign}(e_1)].\end{aligned} \tag{50}$$

We define $\tilde{\beta} = \hat{\beta} - \beta$, $\tilde{\varphi} = \hat{\varphi} - \varphi$, and Eq. (50) can be rewritten as:

$$\begin{aligned}\dot{V} =& -k_1 e_1^2 - k_r r^2 - k_2 e_2^2 + e_1 r - k_2 e_2 r \\ & - \hat{\varphi}|e_2 + r| + \theta_1 \tilde{x}_{e2}(e_2 + r) + \tilde{\varphi}\mathrm{Proj}(e_2 + r) \\ =& -k_1 e_1^2 - k_r r^2 - k_2 e_2^2 + e_1 r - k_2 e_2 r \\ & - \hat{\varphi}|e_2 + r| + \hat{\varphi}\mathrm{Proj}(e_2 + r) \\ & + \theta_1 \tilde{x}_{e2}(e_2 + r) - \varphi\mathrm{Proj}(e_2 + r).\end{aligned} \tag{51}$$

If φ is sufficiently large, we have the following:

$$-\hat{\varphi}|e_2 + r| + \hat{\varphi}\mathrm{Proj}(e_2 + r) \le 0, \tag{52}$$

$$-\varphi\mathrm{Proj}(e_2 + r) + \theta_1 \tilde{x}_{e2}(e_2 + r) \le 0. \tag{53}$$

When Eqs. (52) and (53) are substituted into Eqs. (51), this function is bounded as:

$$\dot{V} \le -k_1 e_1^2 - k_r r^2 - k_2 e_2^2 + e_1 r - k_2 e_2 r \le -e^{\mathrm{T}} \Lambda_1 e, \tag{54}$$

where e is defined as $e = [e_1, r, e_2]^{\mathrm{T}}$, and the matrix Λ_1 defined in Eq. (40) is positive-definite. Therefore,

$$\dot{V} \le -\lambda_{\min}(\Lambda_1)\left(e_1^2 + r^2 + e_2^2\right) \triangleq -W, \tag{55}$$

where $\lambda_{\min}(\Lambda_1)$ is the minimal eigenvalue of matrix Λ_1. Therefore, we can infer that $V \in L_\infty$ and $W \in L_2$, which implies that e_1, r, and e_2 are bounded. Additionally, the states x_1, x_2, and u are bounded. We know that all the error signals of this system are bounded according to Eq. (55). From Assumption 5, we can easily verify that the time derivative of W is bounded and uniform.

Acknowledgements
Not applicable.

Authors' Contributions
JM was responsible for the formulation of the research route and theoretical verification, as well as the formulation of the experimental methods, and wrote the manuscript. JY and WD provided suggestions for revision. All authors read and approved the final manuscript.

Funding
Supported by National Key R&D Program of China (Grant No. 2018YFB2000702), National Natural Science Foundation of China (Grant No. 52075262), and Fok Ying-Tong Education Foundation of China (Grant No. 171044).

Availability of Data and Materials
Not applicable.

Declarations

Ethics Approval and Consent to Participate
Not applicable.

Consent for Publication
Not applicable.

Competing Interests
The authors declare no competing financial interests.

Received: 11 April 2022 Revised: 11 April 2024 Accepted: 11 April 2024
Published online: 27 May 2024

References

[1] L J Jia, H Zhu. *Composite material processing technology*. Tianjing: Tianjin University Press, 2007.
[2] B Wilson. Filament winding - the jump from aerospace to commercial fame. *SAMPE. J.*, 1997, 33(3): 25-32.
[3] H S Li, H Zhu. *CAD/CAM system for filament winding composite material bend pipe*. Zhejiang: Zhejiang University, 2002.
[4] P D Mathur, W C Messner. Controller development for a prototype high-speed low-tension tape transport. *IEEE Transactions on Control Systems Technology*, 1998, 6(4): 534-542.
[5] M D Baumgart, L Y Pao. Robust Lyapunov-based feedback control of non-linear web-winding systems. *42th IEEE Conference on Decision & Control*, Maui, HI, USA, December 9, 2003: 6398-6405.
[6] M D Baumgart, L Y Pao. Robust control of tape transport systems with no tension sensor. *43th IEEE Conference on Decision & Control*, Nassau, Bahamas, December 14, 2004: 4342-4349.
[7] M D Baumgart, L Y Pao. Time-optimal control of web-winding systems with air entrainment. *IEEE/ASME Transactions on Mechatronics*, 2005, 10(3): 257-262.
[8] P R Pagilla, N B Siraskar, R V Dwivedula. Decentralized control of web processing lines. *IEEE Transactions on Control Systems Technology*, 2006, 15(1): 106-117.
[9] J Levine, Choi. Control of roll-to-roll web systems via differential flatness and dynamic feedback linearization. *IEEE Transactions on Control Systems Technology: A Publication of the IEEE Control Systems Society*, 2013, 21(4): 1309-1317.
[10] H Hou, X Nian, S Jing, et al. Robust tension observers design for web-winding systems. *35th Chinese Control Conference* , Chengdu, China, July 27, 2016: 420-425.
[11] J R Dominguez, C Mora-Soto, S Ortega-Cisneros, et al. Copper and core loss minimization for induction motors using high-order sliding-mode control. *IEEE Transactions on Industrial Electronics*, 2012, 59(7): 2877-2889.
[12] G Wang, R Yang, D Xu. DSP-based control of sensorless IPMSM drives for wide-speed-range operation. *IEEE Transactions on Industrial Electronics*, 2013, 60(2): 720-727.
[13] B Xian, D M Dawson, M S Dequeiroz, et al. A continuous asymptotic tracking control strategy for uncertain nonlinear systems. *IEEE Transactions on Automatic Control*, 2004, 49(7): 1206-1211.
[14] J Y Yao, Z X Jiao, D W Ma, et al. High-accuracy tracking control of hydraulic rotary actuators with modeling uncertainties. *IEEE/ASME Transactions on Mechatronics*, 2014, 19(2): 633-641.
[15] J Y Yao, Z X Jiao, D W Ma. RISE-based precision motion control of DC motors with continuous friction compensation. *IEEE Transactions on Industrial Electronics*, 2014, 61(12): 7067-7075.
[16] Z K Yao, J Y Yao, W C Sun. Adaptive RISE control of hydraulic systems with multilayer neural-networks. *IEEE Transactions on Industrial Electronics*, 2019, 66(11): 8638-8647.
[17] J Y Yao, W X Deng, Z X Jiao. RISE-based adaptive control of hydraulic systems with asymptotic tracking. *IEEE Transactions on Automation Science and Engineering*, 2015, 14(3): 1524-1531.
[18] F L Lewis. Neural network control of robot manipulators. *IEEE Expert*, 1996, 11(3): 64-75.
[19] H K Khalil. High-gain observers in nonlinear feedback control. *International Conference on Control, Automation and Systems,* Seoul, South Korea, October 14, 2008: 13-23.
[20] J Q Han. From PID to active disturbance rejection control. *IEEE Transactions on Industrial Electronics*, 2002, 9(3): 13-18.
[21] W H Chen. Disturbance observer based control for nonlinear systems. *IEEE/ASME Transactions on Mechatronics*, 2004, 9(4): 706-710.

[22] S Li, J Yang, W H Chen, et al. Generalized extended state observer based control for systems with mismatched uncertainties. *IEEE Transactions on Industrial Electronics*, 2012, 59(12): 4792-4802.
[23] A Radke, Z Gao. A survey of state and disturbance observers for practitioners. *American Control Conference*, Minneapolis, USA, June 14, 2006: 1-12.
[24] Z Gao, H Yi, J Han. An alternative paradigm for control system design. *40th IEEE Conference on Decision & Control*, Orlando, USA, 2001: 4578-4585.
[25] J Y Yao, Z X Jiao, D W Ma. Extended-state-observer-based output feedback nonlinear robust control of hydraulic systems with backstepping. *IEEE Transactions on Industrial Electronics*, 2014, 61(11): 6285-6293.
[26] J Y Yao, Z X Jiao, D W Ma. Adaptive robust control of DC motors with extended state observer. *IEEE Transactions on Industrial Electronics*, 2014, 61(7): 3630-3637.
[27] J Y Yao, W X Deng. Active disturbance rejection adaptive control of hydraulic servo systems. *IEEE Transactions on Industrial Electronics*, 2017: 1-1.
[28] J Y Yao, W X Deng. Active disturbance rejection adaptive control of uncertain nonlinear systems: Theory and application. *Nonlinear Dynamics*, 2017.
[29] W Xue, W Bai, S Yang, et al. ADRC with adaptive extended state observer and its application to air–fuel ratio control in gasoline engines. *IEEE Transactions on Industrial Electronics*, 2015, 62(9): 5847-5857.
[30] H Liu, S Li. Speed control for PMSM servo system using predictive functional control and extended state observer. *IEEE Transactions on Industrial Electronics*, 2012.
[31] S E Talole, J P Kolhe, S B Phadke. Extended-state-observer-based control of flexible-joint system with experimental validation. *IEEE Transactions on Industrial Electronics*, 2010, 57(4): 1411-1419.
[32] J J Mi, J Y Yao. ESO-based adaptive robust control of 3-axis winding of carbon fiber. *39th Chinese Control Conference*, Shenyang, China, July 27, 2020: 410-415.
[33] J J Mi, J Y Yao, W X Deng. Neural network based RISE control of winding tension. *Journal of Mechanical Engineering*, 2021, 57(24): 75-84.
[34] C Makkar, W E Dixon, W G Sawyer, et al. A new continuously differentiable friction model for control systems design. *IEEE/ASME International Conference on Advanced Intelligent Mechatronics*, Monterey, USA, July 24, 2005: 600-605.
[35] L Q Gaol. On stability analysis of active disturbance rejection control for nonlinear time-varying plants with unknown dynamics. *46th IEEE Conference on Decision and Control*, New Orleans, USA, December 12, 2007: 3501-6.

Junjie Mi born in 1994, is currently a PhD candidate at *School of Mechanical EngineeringNanjing University of Science and Technology, China*. He received his bachelor degree from *Anhui Agricultural University, China*, in 2017. His research interests include servo control of mechatronic and multi-rigid body system, nonlinear compensation, adaptive control.

Jianyong Yao born in 1984, is currently a professor at *Nanjing University of Science and Technology, China*. He received his bachelor degree from *Tianjin University, China*, in 2006, and the PhD degree in mechatronics from *Beihang University, China*, in 2012. He was a visiting exchange student at *School of Mechanical Engineering, Purdue University, U.S.A.,* from 2010 to 2011. His research interests include servo control of mechatronic system, adaptive and robust control, fault detection and accommodation of dynamic system.

Wenxiang Deng born in 1991, is currently a lecturer at *Nanjing University of Science and Technology, China*. He received his bachelor degree from *Central South University, China,* in 2013, and the PhD degree in mechatronics from *Nanjing University of Science and Technology, China,* in 2018. His current research interests include servo control of mechatronic systems, nonlinear compensation, and robust adaptive control.